pubs.acs.org/Biomac

Article

Extracellular Secretion and Simple Purification of Bacterial Collagen from *Escherichia coli*

Zahra Abdali, Max Renner-Rao, Amy Chow, Anqi Cai, Matthew J. Harrington, and Noémie-Manuelle Dorval Courchesne*

Cite This: *Biomacromolecules* 2022, 23, 1557−1568

Read Online

ACCESS | Metrics & More | Article Recommendations | Supporting Information

ABSTRACT: Because of structural similarities with type-I animal collagen, recombinant bacterial collagen-like proteins have been progressively used as a source of collagen for biomaterial applications. However, the intracellular expression combined with current costly and time-consuming chromatography methods for purification makes the large-scale production of recombinant bacterial collagen challenging. Here, we report the use of an adapted secretion pathway, used natively by *Escherichia coli* to secrete curli fibers, for extracellular secretion of the bacterial collagen. We confirmed that a considerable fraction of expressed collagen (~70%) is being secreted freely into the extracellular medium, with an initial purity of ~50% in the crude culture supernatant. To simplify the purification of extracellular collagen, we avoided cell lysis and used cross-flow filtration or acid precipitation to concentrate the voluminous supernatant and separate the collagen from impurities. We confirmed that the secreted collagen forms triple helical structures, using Sirius Red staining and circular dichroism. We also detected collagen biomarkers via Raman spectroscopy, further supporting that the recombinant collagen forms a stable triple helical conformation. We further studied the effect of the isolation methods on the morphology and secondary structure, concluding that the final collagen structure is process-dependent. Overall, we show that the curli secretion system can be adapted for extracellular secretion of the bacterial collagen, eliminating the need for cell lysis, which simplifies the collagen isolation process and enables a simple cost-effective method with potential for scale-up.

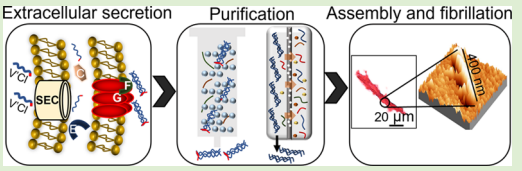

INTRODUCTION

There is a tremendous need for protein-based materials that are derived from safe and biocompatible sources in the fields of biomaterials and tissue engineering. The occurrence of widespread disease among animals and associated health problems inhibits the production and use of animal source proteins. As a consequence, recombinant proteins are emerging as an important substitute that presents lower immunogenicity and inflammation response compared to animal sources.[1] Collagen is among the most abundant proteins in animals, and it plays a major structural and mechanical role in tissue formation. It is thus a protein of choice in different fields such as cosmetics, tissue engineering, and fabricating synthetic biomaterials.[2]

Among the different types of recombinant collagens, bacterial collagen-like proteins, such as Streptococcal collagen-like proteins, have a structure with mechanical and thermal stability compared to type-I animal collagen.[3−5] The biofunctionality of this type of collagen is tailorable and has been genetically modified to alter its biological activities by fusing functional protein domains, such as silk to the C-terminal end of bacterial collagen and single mutations to create integrin-binding domains in the backbone of the bacterial collagen.[6−8]

Bacterial collagen lacks hydroxyproline, which contributes to the stability of animal collagen and cannot be post-translationally modified in bacterial cells. Nonetheless, it still forms a stable triple helix structure.[5] Structurally, bacterial collagen consists of an N-terminal variable domain (globular domain, V) attached to a rod-shaped collagen-like domain (helical domain, CL). A high content of proline and highly charged repeating sequences can be found near the C-terminal and N-terminal ends of the collagenous domain, which are key for the structural stability of the bacterial collagen.[5] Investigations in synthetic peptides have demonstrated that charged residues found in the *X* and *Y* positions of the triplet (glycine-*X*−*Y*) can promote electrostatic interactions and water-mediated contact between the charged side chains, which accordingly stabilize the triple helix structure.[9,10]

Bacterial collagen has been previously genetically modified and produced intracellularly in *Escherichia coli* for biomedical applications.[6−8,11] In these reports, cell lysis has been used as a necessary step for extracting intracellular collagen. However, the extracellular production of proteins has significant advantages compared to conventional intracellular production, on both analytical and industrial scales. For instance, the product quality (e.g., biological activity and stability) of the expressed proteins in

Received: September 11, 2021
Revised: February 22, 2022
Published: March 8, 2022

https://doi.org/10.1021/acs.biomac.1c01191
Biomacromolecules 2022, 23, 1557−1568

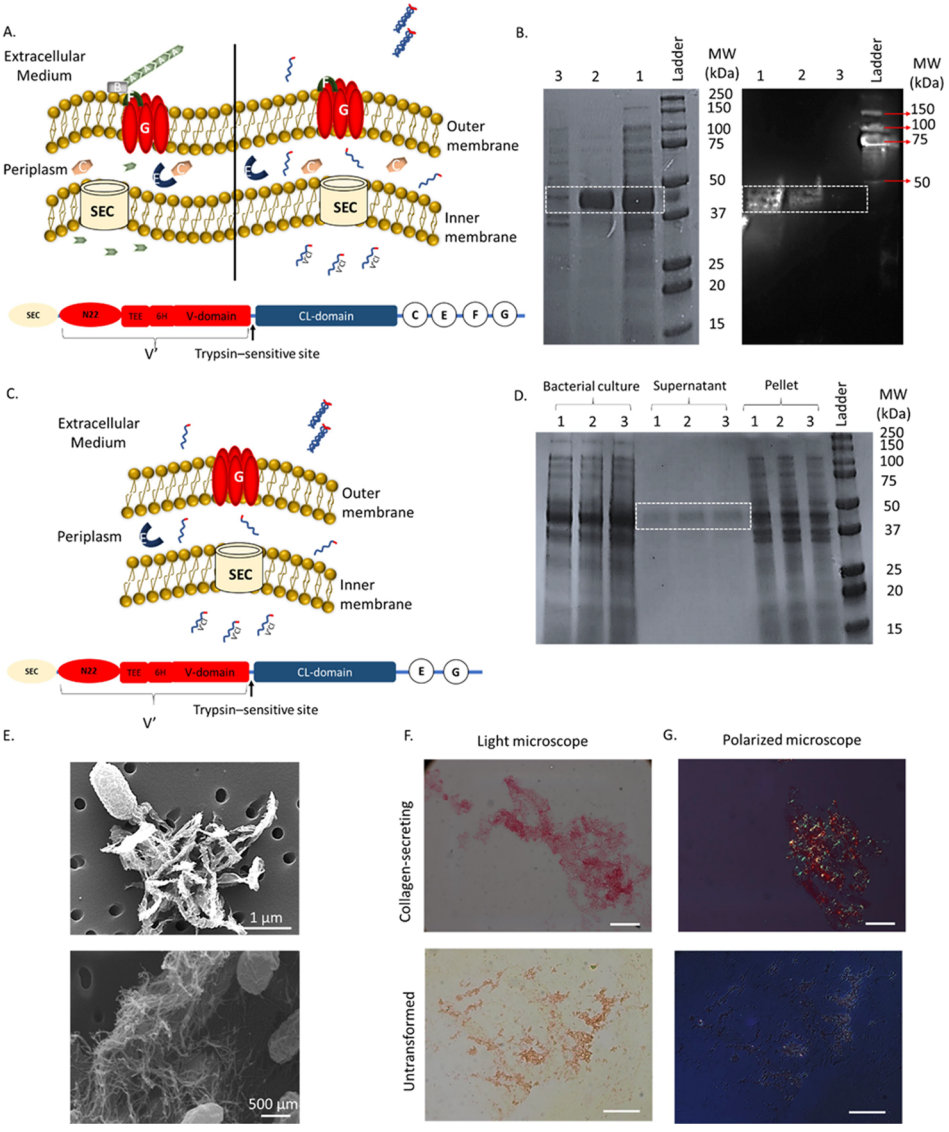

Figure 1. Extracellular secretion of bacterial collagen from *E. coli* cells. (A) Arrangement of the encoding genes of the necessary components for extracellular secretion of the bacterial collagen (bottom) and the existing extracellular secretion pathway for curli fibers consists of SEC, N22, CsgB, CsgA, CsgC, CsgE, CsgF, and CsgG (top, left), and adapted pathway for the secretion of collagen, where CsgB and CsgA are removed (top, right). CsgE and CsgG are necessary for both pathways. (B) Distribution of collagen in the bacterial culture after separation of the pellet and supernatant. Detection of His-tagged collagen in each fraction via western blotting (right) and its representative stained SDS-PAGE gel (left). 1: bacterial culture, 2: supernatant, and 3: pellet. (C) Modified secretion pathway where CsgB, CsgA, CsgC, and CsgF components are removed, and the corresponding gene arrangement. CsgA, CsgB, CsgC, and CsgF are only necessary when secreting curli fibers. (D) Extracellular secretion of collagen in the bacterial culture through the modified pathway shown by SDS-PAGE. Distribution of the collagen in the bacterial collagen after separation of the pellet and supernatant related to the different modified vectors, 1: pET21d-*v′cl-csgCEFG*, 2: pET21d-*v′cl-csgEFG*, and 3: pET21d-*v′cl-csgEG*. (E) SEM images of bacterial cultures expressing collagen, showing extracellular fibrillar structures. (F,G) Observation of secreted triple helical structures from collagen-secreting PQN4 cells. Images of Sirius Red-stained cultures are taken both under the light microscope (F) and polarized light microscope (G). The triple helical structure of the collagen appears red under the polarized light, compared with the untransformed PQN4 cells, indicating that the collagen secreted extracellularly was able to form a stable triple helix. Scale bars: 20 μm.

the culture medium is better preserved by their continuous secretion and protection from intracellular proteolysis by periplasmic proteases.[12] Furthermore, intracellular systems demand cell disruption, which results in protein loss and contamination with host proteins. In contrast, an extracellular system is exempt from cell lysis, which consequently makes the purification process simpler and less costly.[13]

One of the well-known and established extracellular secretion pathways is natively found in *E. coli* bacteria and serves for the secretion of CsgA proteins. CsgA is a self-assembling bacterial protein that is secreted inherently by *E. coli* and assembles into membrane-bound extracellular curli fibers.[14−16] The structural components and assembly apparatus of CsgA consist of seven curli-specific genes (*csg*), which are encoded by two divergently transcribed operons (*csgBAC* and *csgDEFG*). These operons encode the structural subunit of the curli protein and other accessory proteins required for CsgA secretion and assembly.[14]

In the curli secretion pathway, the SEC peptide and N22 peptide are two important components responsible for directing the secretion of CsgA into the periplasm and then across the outer membrane, respectively.[14] These components are not specific to CsgA and are crucial for the extracellular secretion of

https://doi.org/10.1021/acs.biomac.1c01191
Biomacromolecules 2022, 23, 1557−1568

other proteins through this pathway. CsgB is the nucleator protein, and in its absence, CsgA is secreted freely from the cell.[14] The CsgE protein is known as a curli secretion specificity factor that prevents premature amyloid fiber aggregation, and, therefore, is crucial for the secretion of CsgA and CsgA fusion proteins, but also does not interfere with the secretion of proteins containing the N22 secretion signal peptide.[17] CsgF is also responsible for the efficient nucleation of curli subunits into amyloid fibers and acts cooperatively with CsgB to initiate curli subunit polymerization near the cell surface.[18] It has been shown that the CsgG is an ungated, nonselective protein secretion channel in which the periplasmic polypeptides can be transported into the extracellular medium via its diffusion-based mechanism.[19] Additionally, the CsgG transporter is capable of exporting heterologous and non-native sequences, amyloid or not, when fused to the curli subunit CsgA[20] or a truncated form of CsgA.[21] The role of CsgC in this pathway remains to be fully elucidated, but it presumably has redox activity, with CsgG being the potential substrate. Indeed, a mutant strain lacking the *csgC* gene was found to still assemble curli fibers but showing defects in autoaggregation (Figure 1A).[22]

The nonspecificity of the CsgG transporter motivated us to seek inspiration from this existing system for the extracellular secretion of bacterial collagen. Thus, here, we propose an adapted secretion system that can be used for the extracellular secretion of bacterial collagen, using only the essential signal peptides and curli operon genes for the secretion of collagen. The extracellular production of proteins also indirectly permits their simplified purification, which is important for the scalable manufacture of biomaterials. In addition, establishing a low-cost simple purification technique represents an important engineering contribution for the scalable manufacture of protein-based materials.[16] In particular, there are several main drawbacks with current chromatography-based methods, such as high cost, low yield, limited sample volume, and protein loss because of metal ion leakage, which all will limit the massive production of collagen. Therefore, alongside extracellular collagen secretion, we also report simple purification protocols for isolating bacterial collagen, based on three main principles: the enzymatic digestion of the unwanted proteins by selectively cleaving proteins that are sensitive to proteases, the size-based separation of collagen via filtration, and the selective acid precipitation of collagen.[11,23] Through precipitation and filtration, the large culture volumes can be processed and concentrated efficiently, facilitating collagen recovery.

Our work here verifies the hypothesis that the adapted curli extracellular secretion system can be used for the extracellular secretion of bacterial collagen. We also introduce the protocols for simple isolation of the secreted bacterial collagen. We characterize the morphology, secondary structure, and chemical structure of the isolated collagen samples and study their processability for future potential applications in the fields of biomaterials and tissue engineering. This work opens up the opportunity for using bacterial collagen as a major component of biomaterials, relying on the presented simplified secretion and scalable purification methods.

MATERIALS AND METHODS

Cell Strains, Plasmids, and Collagen Expression. The pET21d-*csgACEFG* plasmid and the curli operon deletion mutant strain of *E. coli*, PQN4, were gifts from the Joshi Lab (Harvard University, Boston, MA). We used this pET21d plasmid, with the curli operon (without the CsgB nucleator protein) under the control of the T7 promoter, as a template vector to synthesize the bacterial collagen. On this template vector, we genetically added the encoding genes that are necessary for extracellular secretion of the bacterial collagen and eliminated the *csgA* gene, which encodes the major subunit of the curli fibers, CsgA, and replaced it with a gene encoding bacterial collagen. To do so, first, we linearized the pET21d-*csgACEFG* plasmid using forward and reverse primers starting immediately downstream and immediately upstream, respectively, to remove the csgA gene. Then, the collagen DNA fragment (Life technologies) was inserted downstream of N22 using an isothermal Gibson assembly reaction (New England Biolabs). Also, a translational enhancing element (TEE) encoding the amino acid MNHKVHM was added at the N-terminus of the collagen sequence, which has been shown to enhance translation initiation.[24] The TEE was followed by a six-histidine tag (His-tag) to allow for immunodetection. The templated vector for the secretion system, which consists of the genes expressing SEC, N22, His-tag, and collagen, and the curli-specific genes (*csg*), *csgC*, *csgE*, *csgF*, and *csgG* (pET21d-*v′cl-csgCEFG*), was transformed into *E. coli* PQN4 and BL21(DE3) (New England Biolabs). In another approach, we also deleted *csgC* and *csgF* to further investigate their effect on the extracellular secretion of the bacterial collagen (pET21d-*v′cl-csgEFG* and pET21d-*v′cl-csgEG*).

Figure 1A demonstrates the arrangement of the encoding genes on the template vector. To express the proteins, the transformed PQN4 cells were streaked onto lysogeny broth (LB) agar plates containing 100 μg/mL carbenicillin and 0.5% (m/v) glucose (for catabolite repression of T7 RNA polymerase). Colonies were picked from the plates, and 5 mL cultures were inoculated in LB medium (containing 100 μg/mL carbenicillin and 2% (m/v) glucose). Cultures were grown overnight at 37 °C with an agitation rate of 250 rpm. The overnight cultures were diluted 100-fold in fresh LB medium with 100 μg/mL carbenicillin, and protein expression was allowed to proceed at 37 °C overnight. The protein sequence of the bacterial collagen and DNA sequences of all the genes and primers are listed in Table S1.

Assessment of Collagen Expression, Purity, and Secretion by Sodium Dodecyl Sulfate-Polyacrylamide Gel Electrophoresis (SDS-PAGE) and Western Blotting. We confirmed the expression of His-tagged collagen and its secretion into the culture medium by running an SDS-PAGE gel of different fractions of the culture and detecting collagen via western blotting. We used three samples; a 30 μL sample taken from a 5 mL freshly expressed culture, a supernatant (30 μL), and washed bacterial pellets (30 μL). To prepare the pellets, we centrifuged 1 mL of the culture, removed the supernatant, and after one wash with HCl 0.05 M, and two washes with water, they were resuspended with 1 mL water. We ran all samples on a NuPAGE Novex 4−12% Bis-Tris gel and transferred them on an iBlot PVDF membrane (Invitrogen). We treated the membrane with a monoclonal mouse anti-His antibody, the HRP conjugate (Abcam), after blocking with 5% milk in TBST. We detected the chemiluminescence using a FluorChem M system (Protein Simple). We used ImageJ to calculate the intensity of the bands by quantifying the bands corresponding to the supernatant and pellets relative to the intensity of the band corresponding to the culture.

We also loaded the same samples on TGX gel and stained them with Coomassie Blue for more assessment along with the western blot results. We also used SDS-PAGE to assess the purity of the purified collagen samples and confirm their molecular weights. After resuspending 30 μL of the purified collagen solution (5 mg/mL) in 10 μL 4× Laemmli loading buffer, it was loaded in every 50 μL wells of a precast Mini-Protean TGX gel (Bio-Rad Laboratories). The gels were electrophoresed at 200 V for 30 min and then stained with Coomassie Blue.

Assessment of Collagen Expression, Secretion, and Folding by Sirius Red Staining. The supernatant of the collagen-expressing culture was stained with Sirius Red and Masson's trichrome and was compared with the supernatant of a nontransformed PQN4 culture, as control. For Sirius Red staining, ∼10 μL of the supernatant were air-dried on a glass slide for 5−10 min and were heat-fixed by gently passing the slides over a flame. The slides were immersed for 1 h in saturated picric acid containing 0.1% Direct Red 80 (i.e., Sirius Red, Sigma) and washed with 0.5% acetic acid (twice for 2 min). The slides were

https://doi.org/10.1021/acs.biomac.1c01191
Biomacromolecules 2022, 23, 1557−1568

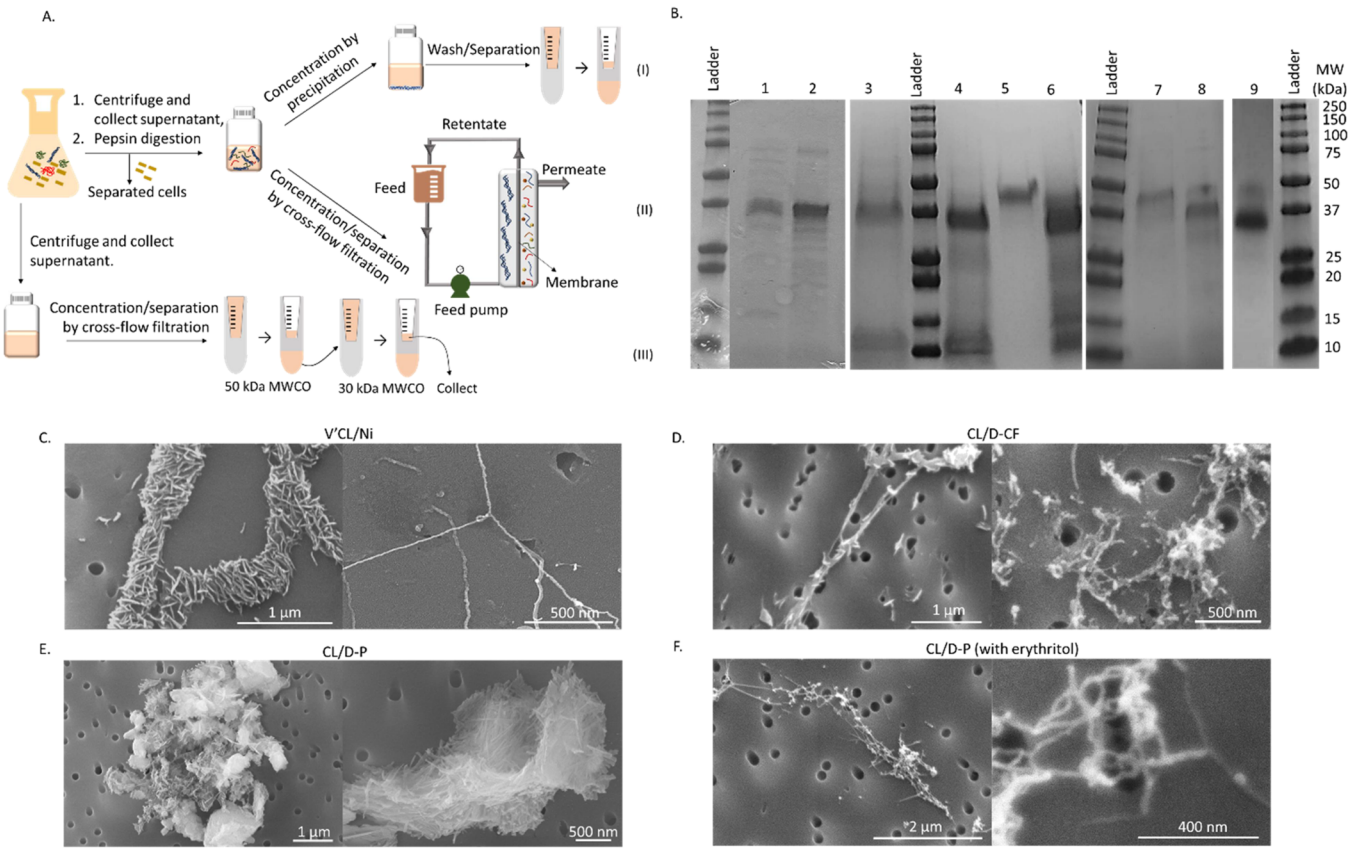

Figure 2. Purification of extracellular collagen using scalable methods. (A) Scheme of two scalable purification methods: digestion/precipitation or (D−P, top) and digestion/cross-flow filtration (D−CF, bottom). After the filtration, the collagen domain (CL) will be trapped in the retentate and the digested variable domain (V′) and other small digested proteins will be removed through the permeate. The supernatant is first separated from bacterial cells via centrifugation and digested with pepsin. It is then subjected to separation via precipitation or filtration. (B) SDS-PAGE analysis of the purified collagen samples showed comparable purity with collagen/Ni and no fragmentation during the purification; supernatant of the bacterial culture expressed in PQN4 and BL21d (1 and 2), pepsin-digested supernatant (3), CL/D−P (4), V′CL/Ni (5), CL/D−CF (6), V′CL/CF (7) CL/D−P, and CL/D−CF and (washed with 30 kDa centrifugal filters to remove the remaining impurities) (8 and 9). (C−F) Morphology of the purified proteins observed by SEM; (C) purified collagen by chromatography (V′CL/Ni) showing the nano/microsized fibers, (D) CL/D−CF kept its integrity and fibrillar structure after purification, (E) aggregated structure of the collagen obtained from D−P method, and (F) collagen obtained from the D−P method and protected by erythritol, showing an intact fibrillar structure comparable with V′CL/Ni.

dehydrated by increasing concentrations of absolute alcohol (95, 100, and 100%) each for 2 min followed by a xylene wash and mounted in Neo-Mount resin (VWR). Birefringence images of the stained samples were taken using a polarized light microscope (Axio Scope.A1, Zeiss) equipped with a six-megapixel CCD camera (Axiocam 505 color, Zeiss). We used rat tail collagen (Sigma-Aldrich) as a control for type-I animal collagen. We also stained the purified collagen samples with Sirius Red to study the effect of the purification process on their structures.

For Masson's trichrome (Sigma-Aldrich) staining, the manufacturer's protocol was followed. Briefly, the samples were stained for 5 min stepwise in separate solutions of Weigert's iron hematoxylin, Biebrich scarlet-acid fuchsin, phosphomolybdic-phosphotungstic acid, and aniline blue. The same steps as those for Sirius Red staining were followed for washing, dehydrating, mounting, and imaging.

Purification of Collagen Proteins Using the Ni-NTA Column. We used the Ni-NTA column for collagen purification as a gold-standard method. To do so, we first filtered the collected supernatant through 0.2 μm bottle filters (Thermo Fisher) to remove the large particulates and possible remaining bacteria. We incubated the Ni-NTA column with the supernatant for 2 h, washed it with 40 mM imidazole solution five times to remove the nonspecifically bound proteins, and washed it with 500 mM imidazole solution to elute the bound proteins. Then, the eluate was concentrated and washed with a 30 kDa Pall centrifugal filter. To remove the non-collagenous domain (V′), the purified protein was adjusted to pH = 2.2 with HCl 0.5 M and incubated with trypsin (0.01 mg/mL) for 24 h at 4 °C. To stop the digestion, the pH was adjusted with 0.5 N NaOH to pH 8.0, and the protein solution was washed through a 10 kDa Pall centrifugal filter. Abbreviations of the samples are listed in Table S2.

Isolation of Collagen Proteins Using Digestion/Cross-Flow Filtration. We collected the supernatant by 30 min centrifugation at 4000× *g*. After filtering the supernatant through 0.2 μm bottle filters, we lowered the pH to 2 (optimum pH for pepsin function[25]), added pepsin to the supernatant at a final concentration of 0.01 mg/mL, and incubated it at 4 °C overnight for pepsin to digest the pepsin-sensitive impurities. Next, we concentrated the voluminous crude protein solution by cross-flow filtration. We used a Minimate tangential flow filtration system (Pall Life Sciences) to filter 500 mL of the digested supernatant through a 10 kDa molecular weight cut-off (MWCO) membrane. The permeate containing small solutes and digested proteins were discarded, and the concentrated retentate (containing collagen) was collected as the product (Figure 2A). The retentate was further washed with 500 mL of 10 mM sodium phosphate buffer pH = 7.4.

Isolation of Collagen Proteins Using Digestion/Precipitation. Another approach to concentrate the large volume of the digested supernatant was acid precipitation. We used phosphotungstic acid (PTA), at a final concentration of 0.1%, to precipitate the digested and nondigested proteins (collagen) from 100 mL supernatant. To prevent the denaturation of the collagen structure during acid precipitation, we added erythritol (0.5 M) to the protein solution and incubated it on ice

https://doi.org/10.1021/acs.biomac.1c01191
Biomacromolecules 2022, 23, 1557−1568

for 2 min (Figure 2A). After collecting the precipitated proteins by centrifugation at 4000 × *g* for 5 min, we washed the precipitates with 5 mL acetone twice and air-dried them for 30 min. Then, the precipitate was resolubilized in 10 mL NaOH (0.05 N) and washed with a 10 kDa centrifugal filter (Pall) to remove the remaining small-size digested impurities from the final product. After the isolation process, the collected purified collagen solution (1 mL) was further washed with 10 mM sodium phosphate buffer pH = 7.4 with the centrifugal filter and lyophilized.

Electron Microscopy. Samples for scanning electron microscopy (SEM) were prepared by depositing 50 μL of the freshly expressed bacterial culture and the purified collagen samples on 0.2 μm polycarbonate filter membranes (Whatman Nuclepore from Millipore Sigma). The membranes were washed with 0.1 M sodium cacodylate buffer (Electron Microscopy Sciences), fixed with 2% (v/v) glutaraldehyde (Bio Basic) and 2% (v/v) paraformaldehyde (Electron Microscopy Sciences) for 2 h at room temperature, and solvent-exchanged sequentially in 0, 25, 50, 75, and 100% (v/v) ethanol (for 15 min in each solvent). The membranes were dried in a critical point dryer and sputtered with 5 nm Pt. Imaging was performed using an FEI Quanta 450 ESEM at 5 kV.

Nanostructure of the Collagen Fibril. Atomic force microscopy (AFM) was used to study the nanostructure of self-associated collagen fibers; 0.5 mg of the collagen purified via Ni-NTA chromatography was resolubilized in 1 mL of 1 mM phosphate buffer at pH = 7.4. The collagen solution was incubated at 37 °C for 1 h to facilitate the fibrillogenesis and self-association of the collagen fibrils. Then, 4 μL of the protein solution was added onto a freshly cleaved mica sheet and was allowed to dry overnight. The samples were imaged using a Veeco Multimode Nanoscope III AFM with a 240 AC-NA microcantilever tip (Opus).

Circular Dichroism (CD) Spectroscopy. A Chirascan spectrophotometer (Applied Photophysics) was used to evaluate the secondary structure of the engineered proteins. Measurements were performed in a quartz cell with a 1 mm path length from 180 to 260 nm at 20 °C, using a 1 nm step size and a bandwidth of 1 nm. The protein solutions were prepared by dissolving 0.5 mg of the proteins in 1 mL of water followed by 30 s vortexing to fully dissolve the proteins. All spectra were baseline-corrected with respect to water. Also, using a Jasco J-815 CD spectrophotometer the protein melting was monitored at 198 nm by increasing temperature in 1 °C increments from 5 to 50 °C, at pH = 5. Proteins were maintained for 1 min at each temperature, with the average rate of temperature increase of 1 °C/min.

Polarized Confocal Raman Spectroscopy. Confocal Raman spectroscopy of the collagen samples was performed under dry conditions after casting the protein solutions onto glass slides. A green laser (Nd/YAG laser, λ = 532 nm) was focused using a confocal Raman microscope equipped with a motorized scanning stage (Alpha300R, WItec, Ulm, Germany). The scattered light was detected by a thermoelectrically cooled CCD detector (Andor, Belfast, North Ireland) placed behind the spectrometer (WItec). Using a 100× objective (Zeiss, NA = 0.9), individual point scans of vesicles contained large contributions from the surrounding glass and dried buffer; therefore, image scans were performed with a laser power of 27 mW, polarization angles of 0° (perpendicular to major axis) and 90°(parallel to major axis), and an integration time of 1.5 s per point.

Processing of Collagen Samples. To test the potency of the collagen for being used in different forms for biomaterial applications, collagen was processed in the forms of free-standing films and hydrogel crosslinked with genipin, a naturally derived chemical crosslinker. To form the collagen films, a collagen solution (10 mg/mL) in 0.01 M acetic acid was incubated at 4 °C overnight, cast on glass slides, and air-dried overnight. An aqueous solution of collagen (5 mg/mL) was crosslinked by mixing with a solution of genipin (Abcam) in DMSO:PBS (1:3) with final concentrations of 2.5 and 5 mM. The collagen−genipin mixture was incubated at 37 °C overnight. To induce the gelation of the collagen, an aqueous solution of collagen (5 mg/mL) was incubated with 2.5% sodium dodecyl sulfate (SDS) at 37 °C overnight.

UV−vis analysis was used to confirm crosslinking by observing a characteristic absorption peak at 585 nm. Because genipin also endows the crosslinked proteins with an intrinsic fluorescence, the fluorescence properties of the genipin-crosslinked hydrogels were studied using a fluorometer (Thermo Fisher). The excitation wavelength was 590 nm, and emission spectra were collected from 600 to 700 nm. To assess the effects of SDS and genipin on the rheological properties of the collagen, we measured the viscosity of the samples at different shear rates using an Anton Paar MCR 302 rheometer. The measurements were operated with a 12 mm diameter cone-plate geometry (CP12). To prevent evaporation, the rheometer was equipped with a temperature-controlled hood; 200 μL of the samples were carefully placed onto the surface of the lower plate, and the upper cone was lowered to a 0.5 mm gap distance. Before testing, the hydrogels were resting for 2 min to equilibrate their mechanical stability. During the amplitude sweeps, the frequency was kept constant at 1 rad s^{-1}. The frequency sweep was conducted from 10 to 1 rad s^{-1}.

Results and Discussion. **Expression and Extracellular Secretion of Bacterial Collagen.** After transforming the bacteria, we sought to determine whether collagen could be expressed and secreted extracellularly as expected through the curli secretion pathway. To do so, we searched for the presence of His-tagged collagen in the whole bacterial culture, in the supernatant only, and in the bacterial pellet only, using SDS-PAGE and western blotting (Figure 1B). In the culture and supernatant, we observed a band close to the expected molecular weight of the bacterial collagen (∼34 kDa), which consists of the N-terminal variable domain plus N22 (V′), TEE, His-tag, trypsin-sensitive region (for selective isolation of the collagen domain), and collagen domain (CL) (Figure 1B, lanes 1 and 2). This band was slightly higher (∼ 44 kDa) than the theoretical molecular weight of the construct, which is common for rod-shaped proteins.[26] The intensity of this band extracted from the pellet was weak and hard to distinguish (with an intensity of less than 1% of that of the whole culture), which indicates that the fraction of bacterial collagen that remains trapped inside the cells is negligible (Figure 1B, lane 3). As expected, the intensity of the band in the supernatant fraction was significantly higher (∼70% of the intensity of the whole culture). Thus, after expression, a considerable fraction of the collagen (∼70%) is being secreted freely in the extracellular medium. The remaining fraction (∼30%), while not present in the washed pellet, may remain weakly associated with the pellet before washing with dilute hydrochloric acid and water. This extracellular, but pellet-associated collagen does not appear on the gels because the pellet that was run was washed. As a control for the pET21d vector and the secretion pathway, we used pET21d-MBP (maltose binding peptide, a 42.5 kDa soluble protein) and ran an SDS-PAGE for the fractions from the culture, supernatant, and pellet (Figure S1A). The control showed that in the absence of the curli secretion pathway, no MBP was secreted into the extracellular medium. We also looked at the molecular weight of the proteins in the culture from untransformed PQN4 cells (control for the transformed cells) which indicated no protein corresponding to our protein of interest (collagen) (Figure S1A).

Taken together, these observations indicate that the supernatant can be used in subsequent purification processes and can readily enable the recovery of more than 70% of the expressed collagen. Our observations also imply that the curli secretion pathway is not specific to the secretion of CsgA proteins,[19,20] and is instead compatible with the secretion of other proteins that are not CsgA, CsgA-like, or fused to CsgA, such as collagen. Indeed, the N-terminal fusion of the SEC and N22 peptides was sufficient to ensure the efficient secretion of collagen.

We further modified the secretion pathway by removing *csgC* and *csgF* genes, and we assessed the secretion of the collagen into the extracellular medium using SDS-PAGE (Figure 1C,D) and western blotting (Figure S1B). Similar to the unmodified pathway (pET21d-*v′cl-csgCEFG*), the modified secretions pathways lacking CsgC and CsgF proteins were able to direct the collagen into the extracellular media (Figure S1B). The results indicate that collagen is secreted into the extracellular medium even in the absence of CsgC and CsgF. A sharp band at around 44 kDa was observed for all three modified pathways (pET21d-*v′cl-csgCEFG*, 2: pET21d-*v′cl-csgEFG*, 3: pET21d-

https://doi.org/10.1021/acs.biomac.1c01191
Biomacromolecules 2022, 23, 1557−1568

v′cl-csgEG (Figure 1D, lanes 1, 2, and 3). In addition, the presence of the collagen was detected in the supernatant for all samples, indicating constant levels of extracellular secretion. This observation indicates that CsgC and CsgF are not necessary components for the extracellular secretion of the bacterial collagen, a principle which we postulate could be generalized to other non-CsgA proteins secreted via this pathway.

Additionally, we confirmed the presence of assembled collagen in bacterial cultures after expression using SEM. Figure 1E shows extracellularly secreted collagen (alongside an *E. coli* cell) and its fibrillar morphology, after self-associating into fiber meshwork in the bacterial culture. The presence of these self-assembled collagen fibers and aggregates directly in the bacterial culture suggests that collagen molecules begin forming fibrils and bundle into networks immediately after expression and secretion.

To further visualize the secretion of triple helical structures into the extracellular medium, we stained the supernatant of cultures expressing collagen using Sirius Red and Masson's trichrome dyes and compared them with cultures prepared with untransformed PQN4 cells (Figure 1F,G). Fibrillar collagen is highly anisotropic and forms a complex with Sirius Red that enhances the birefringence observed with polarized light microscopy, which can allow distinguishing collagen from non-collagenous proteins.[27] Moreover, the presence of basic amino acids in collagen makes the interaction with the dye stronger.[28] Under unpolarized light, stained fibrillar collagen is expected to appear red. Light microscopy of Sirius Red-stained samples revealed that untransformed PQN4 culture appeared orange, while the supernatant collected from collagen-secreting culture appeared pink-red (Figure 1E). Under polarized light, fibrillar collagen stained with Sirius Red typically exhibits strong birefringence in a range of colors, from yellowish-orange to orange-red. Here, we observed these colors for the collagen-secreting culture only, and not for untransformed PQN4 cells, indicating that the presence of extracellular collagen-like structures in PQN4 cells transformed with the pET21d-*v′cl-csgCEFG* (Figure 1F). The area with the bright yellow/orange color indicates larger and denser aligned collagen fibers (Figure 1F, top). In addition, we stained the supernatant of cultures expressing collagen corresponding to pET21d-*v′cl-csgEFG* and pET21d-*v′cl-csgEG* using Sirius Red (Figure S2). The stained samples appeared red in light microscopy indicating positive staining for collagen and showed birefringence in polarized light microscopy indicating alignment of the collagen molecules. Staining the samples with Masson's trichrome dye also revealed positive staining for collagen. With this method, collagen is expected to produce a blue color while other noncollagen components usually appear in red, pink, brown, and black.[29] The supernatant of the collagen-expressing culture appeared intense blue after staining, compared with untransformed PQN4 cells, which appeared pink (Figure S3). Together, these observations consistently indicate the presence of collagen in the extracellular medium of transformed cells.

Isolation of Secreted Collagen and Its Process-Dependent Morphology. Because collagen is secreted into the extracellular medium, its isolation does not require cell lysis, and collagen can be directly purified from the supernatant. After collecting the supernatant, we isolated collagen using three primary methods: (1) affinity chromatography with Ni-NTA, along with two scalable methods, (2) size-based separation via cross-flow filtration, and (3) collagen precipitation with PTA. These scalable methods can be preceded by a pepsin digestion step to digest protease-sensitive proteins in the supernatant (except the collagen, which is resistant to pepsin digestion) and facilitate subsequent purification steps. They are then performed in a fairly quick manner, using simple size-based separation techniques (filtration and centrifugation). With these methods, 1 L of pepsin-digested supernatant could be purified in a 2-hour purification process. Notably, purification via precipitation also allows for considerably reducing the sample volume at an early stage in the process, from a large bacterial culture down to a few milliliters of product which can easily be lyophilized. Compared with the time that Ni-NTA purification takes (~1 h to purify 10 mL supernatant), this high productivity is an advantage for the scalable manufacture of biomaterials.

We aimed at comparing the purity and structure of the collagen products isolated from scalable methods with those of collagen obtained from well-established Ni-NTA purification. After purification by the three introduced methods (Figure 2A), we verified the purity of the products using SDS-PAGE (Figure 2B). We compared the purity of the collagen samples obtained from pepsin digestion followed by precipitation (D−P) and from pepsin digestion followed by cross-flow filtration (D−CF) with the collagen obtained from Ni-NTA chromatography (V′CL/Ni). SDS-PAGE of the collected crude supernatant (without digestion or purification) showed a strong band for collagen with an initial approximate purity of 45−50%. This relatively high initial purity in the crude supernatant is because no cell lysis is needed for the extraction of collagen, preventing the release of intracellular proteins. We have made this observation for both collagens expressed in PQN4 cells and BL21 cells (Figure 2B, lanes 1 and 2, respectively). In all of the digested samples, we observed a band corresponding to the helical domain of bacterial collagen (CL domain) at around 23 kDa (Figure 2B, lanes 3, 4, 6, 8, and 9). During the digestion step, the nonhelical portions of the collagen construct, which are susceptible to protease digestion, were cleaved, while the helical domain (CL) remained intact with no cleavage or digestion during the purification process. After the pepsin digestion, the bands corresponding to impurities at higher and lower molecular weight than the CL domain (23 kDa) were diminished and an intense band at around 12 kDa appeared, showing the digested impurities (Figure 2B, lane 3). The purity of the collagen obtained from Ni-NTA (Figure 2B, lane 5) was relatively higher than that from the two other purification methods (Figure 2B, lanes 4 and 6−9) and indicated no nonspecifically bound impurities to the Ni-NTA column. To remove low-molecular-weight proteins after purification, we employed centrifugal filters with 10 or 30 kDa MWCO. When a 10 kDa centrifugal filter was used, we still observed a band corresponding to the ~12 kDa V′ fragment comprising N22, the nonhelical domain, and the His-tag (Figure 2B, lanes 4 and 6). This band disappeared when a 30 kDa centrifugal filter was used (Figure 2B, lanes 8 and 9). We also tested the purity of the crude culture supernatant that was not exposed to pepsin digestion but only filtered with a 50 and 30 kDa MWCO centrifugal filter (V′CL/CF, Figure 2B, lane 7). In the first step, impurities with a size greater than 50 kDa were trapped in the filter, and in the second step, impurities with a size smaller than 30 kDa passed through the filter while the product was retained. Because the impurities were not digested, the purity of the V′CL/CF (~70%) was lower than that of the samples purified by other purification methods. In this sample, the purity improved in comparison with the crude supernatant (Figure 2B, lanes 1 and 2), which means that by simply filtering the supernatant an adequate purity may be obtained for the collagen depending on the application.

We then compared and quantified the purity of the collagen products obtained with each method. Ni-NTA yielded a collagen product with almost 100% purity, without any protein impurities visible on SDS-PAGE (Figure 2B, lane 5), and with a ~ 0.5 g/L yield. Indeed, this highly selective Ni-NTA column enabled retention of only the His-tagged proteins (Figure S4). In comparison, we obtained a purity of ~90% for CL/D−CF samples when washed with 30 kDa filters (Figure 2B, lane 7), with a yield of ~0.4 g/L. While the yield for collagen purified via cross-flow filtration is comparable and even slightly lower than that for chromatography purification, cross-flow filtration is a technique that is more suitable for scale-up, could easily be adapted to isolate collagen for large culture volumes, and could be used in a continuous process. Finally, the purity of the CL/D−P sample was ~60 and ~80%, when washed with 10 and 30 kDa filters, respectively (Figure 2B, lanes 4 and 8). We observed a lower yield for the latter (60 mg/L) compared with the filtration method. This can be explained by the fact that acid precipitation does not result in the precipitation of all protein contents in the supernatant, thus yielding fewer products. Although fewer protein impurities appeared in the collagen/Ni sample, it is a tedious and time-consuming process in which both the high cost and trace of Ni ions in the final purified product have been an enormous concern in other collagen-based biomaterials.[30]

Finally, we compared the morphology of collagen isolated with the three purification methods via SEM (Figure 2C−F). V′CL/Ni samples showed nanosized and microsized assembled fibrils (Figure 2C). In some sections of the sample, we could also recognize collagen

https://doi.org/10.1021/acs.biomac.1c01191
Biomacromolecules 2022, 23, 1557−1568

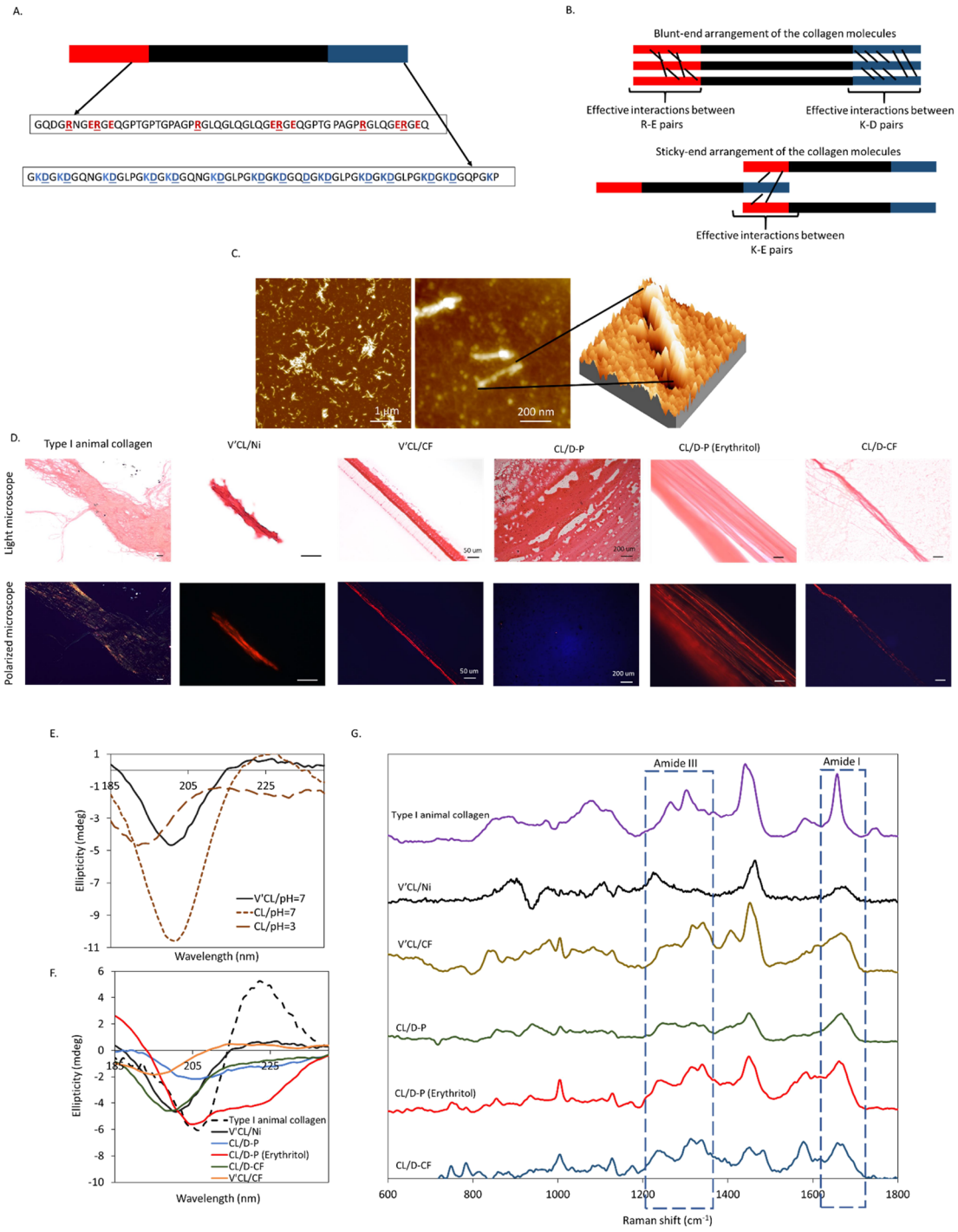

Figure 3. Structure and triple helix formation of bacterial collagen. (A) Scheme showing the collagen domain containing many charged residues such as E−R and K−D at the N- and C-terminal ends, respectively. (B) Schemes showing the blunt-end (top) and sticky-end (bottom) arrangement of the collagen molecules as a result of interactions between the charged amino acid. (C) Individual extended collagen fibers were observed with AFM. One side of the square is 400 nm long. (D) Purified collagen samples and type-I animal collagen strongly bound with Sirius Red and appeared red under the polarized light, indicating the formation of the triple helix (Unlabeled scale bars: 20 μm). (E) Low pH decreased the ellipticity value at 220 nm and therefore affected the stability of the collagen domain. (F) CD spectra were used to study the secondary structure of the bacterial collagen purified with different methods. (G) Raman spectra of the purified collagen highlighting the amide I and amide III bands.

molecules that formed highly ordered networks with pore structures. For samples obtained via cross-flow filtration, we could still distinguish fibrillar structures and a meshwork of fibers (Figure 2D). However, when using the precipitation method, the fibrillar structure of the collagen appeared to have been affected by the acid treatment (Figure 2E). It has been found that the ideal pH value for the formation of native type fibrils is in the range of 5.0 to 8.5. The interaction of PTA with collagen molecules can rupture hydrogen bonds and electrostatic interactions throughout the collagen fibrils, therefore disordering its fibrillar structure.[31] However, when adding erythritol as the protecting agent during precipitation, the collagen structure was preserved by erythritol against low pH (Figure 2F). Indeed, the presence of polyols can preserve the electrostatic interactions that are important for the fibrillogenesis of the collagen. Polyols strengthen the bridge

https://doi.org/10.1021/acs.biomac.1c01191
Biomacromolecules 2022, 23, 1557−1568

interactions between polypeptide chains and replace the water molecules, thereby preserving hydrogen bonds in the backbone of the collagen.[32] The preservation of the highly ordered fibrillar structure of collagen after purification is crucial in employing the final bacterial collagen product to design functional biomaterials. The biomimetic triple helical fiber meshwork with a porous structure obtained from isolated bacterial collagen makes this material an appropriate candidate for restorative biomaterials and tissue engineering applications, where cell integration and diffusion of nutrients are key parameters.[33]

Structural Organization of Bacterial Collagen Proteins. Bacterial collagen triple helix formation and stability are mainly dependent on the electrostatic interactions between the charged amino acids, interactions of the polar residues between several GQN repeats, and the ordered hydration network involved in the numerous polar and charged residues in this domain.[5] In bacterial collagen, 30% of the amino acids in the collagen domain are charged residues, which is 2-times more than the content of charged residues in type-I animal collagen. Near the C-terminal end of bacterial collagen, a domain contains three full repeats of sequence GKD-GKD-GQN-GKD-GLP and several partial repeats of this sequence (Figure 3A, red portion).[5] The effect of charged residues, such as lysine (K) and aspartate (D), on the formation and stabilization of triple helix has been previously studied in collagen-like peptides.[9,34,35] Because of the formation of salt-bridged hydrogen bonds by K−D charge-pairs, these residues are sufficient to form a stable triple helix.[9] In addition to the remarkable role of K−D charge-pairs at the C-terminal, there are a noticeable number of glutamate (E) and arginine (R) residues at the N-terminal of the collagen domain (Figure 3A, blue portion). Investigations in synthetic peptides have demonstrated that relatively stable triple helixes can be produced when these residues are found in the *X* and *Y* positions of the triplet, respectively.[36] Therefore, the R−E pairs at the N-terminal of the collagen can favorably interact via electrostatic attractions and strengthen the triple helix formation throughout the collagen molecules. In a model suggested by Sarkar et al.,[34] it has been shown that a stable triple helix can be formed by the K−D charge-pairs when the positively charged residue (K) at position *X* of the leading strand is paired with the negatively charged residue (D) at position *Y* of the middle strand, one triplet displaced toward the C-terminus. Similarly, the middle strand can interact with the lagging strand and the lagging strand can couple with the leading strand. Figure 3B (top) shows the final assembled triple helix directed by K−D and R−E that forms a "blunt-end" triple helix.[34,37]

Another possible interaction that could result in a different arrangement between the collagen molecules is between K and R (N-terminal end of one molecule with the C-terminal end of another molecule). Hulgan et al.,[38] reported a faster formation of an isopeptide bond between K and E compared with K−D pairs during self-assembly of the collagen mimetic peptides. Therefore, this potential electrostatic interaction can also direct the triple helix self-assembly and eventually result in a "sticky-end" arrangement, in another model suggested by Leary et al., (Figure 3B, bottom).[34,37] The possible sticky-end model in triple helix formation of the collagen can result in the creation of overhangs that extend the length of the triple helix. Theoretically, a single molecule of bacterial collagen is around 60 nm in length, which is 5 times shorter than type-I animal collagen. The suggested sticky-end arrangement for the bacterial collagen can result in indefinite triple helical elongation.

We verified this hypothesis using AFM and observed that the length of collagen can attain a wide range of values from 100 to 500 nm that appeared to be around 45 nm thick, possibly as a result of triple helical elongation as well as lateral packing of the collagen molecules (Figure 3C). However, a range of longer fibrils that bundled together also appeared in the SEM images. Furthermore, the extension can drive the fiber growth more extensively and form long uniform fibers, as we observed by staining purified collagen fibers with Sirius Red (Figure 3D). Upon Sirius Red staining, the bacterial collagen samples (V′CL/Ni, V′CL/CF, CL/D−CF, and CL/D−P (erythritol)) appeared orange-red under the polarized light, similar to animal collagen, indicating the presence of a triple helical structure. The presence of a stained collagen bundle of 80 μm in length and 3 μm in width confirms that the collagen molecules are capable of elongating and bundling into a population of nanofibers with triple helical packing similar to that of type-I animal collagen. As expected, animal collagen appeared as larger bundles compared with bacterial collagen, which is likely due to the larger size of the animal collagen molecule (∼ 1000 amino acids) compared with bacterial collagen (∼200 amino acids). Consistent with the SEM images, integrated fiber-like structures were observed for the purified collagen samples. The collagen samples purified with the filtration method (V′CL/CF and CL/D−CF) both showed fine aligned fibers bound with Sirius Red, which indicated no adverse effect of pepsin digestion on the integrity of the collagen (Figure 3D). However, acid-precipitated collagen (CL/D−P) showed no birefringence under the polarized light, likely because of the denaturation of the collagen structure during acid treatment. However, upon protection by erythritol, the collagen apparently preserved its fibrillar structure, and we observed red bundles indicating the presence of triple helix.

In addition to Sirius Red staining, we studied the formation of triple helical protein secondary structures in bacterial collagen after expression and purification using CD spectroscopy (Figure 3E,F). The CD spectra of the V′CL/Ni at pH = 7 showed a maximum value near 220 nm and a minimum near 200 nm (Figure 3E). The positions of the maximum and minimum peaks demonstrate the characteristic spectrum of triple helical collagen similar to type-I animal collagen, but with lower peak magnitudes. We also note that the CD spectrum of the V′CL showed a lower ellipticity at 220 compared with the isolated collagenous domain (CL), because of the presence of the helical noncollagenous domain (V′) in the V′CL sample (Figure 3E).[5]

We also evaluated the secondary structure of the collagen samples purified from scalable methods (Figure 3F). The most similar spectrum to V′CL/Ni was the spectrum of the V′CL/CF, the sample purified by cross-flow filtration (50 and 30 kDa) of the supernatant, without any treatment. V′CL/CF showed a positive ellipticity value at around 220 nm and a negative value at around 190 nm. A lower ellipticity value in this sample compared with V′CL/Ni was probably due to the presence of the impurities (purity 70% according to the SDS-PAGE result (Figure 2B)). The shape of the spectrum for CL/D−CF was similar to that for V′CL/Ni, but with a lower ellipticity value at 220 nm, which could be due to a slight dissociation of the collagen molecules, potentially caused by the low pH necessary for the activity of the pepsin enzyme used in the digestion step (which precedes cross-flow filtration and precipitation purification, but not chromatography purification). We observed more pronounced differences in the CL/D−P spectrum. The positions and magnitude of the maximum and minimum peaks in the CL/D−P differed from those for V′CL/Ni. The pepsin and acid treatment likely caused the loss of the triple helix structure and the emergence of a random coil (denatured) structure.[39] Also, because the V domain in these samples is susceptible to digestion, they are more prone to incomplete folding, as the V domain helps with self-association and folding of the CL domain.[40] However, protecting the collagen with erythritol resulted in a less pronounced collagen denaturation, but strikingly, in an increase in its alpha-helical content based on distinct minima at around 205 and 220 nm.[41] These results are in accordance with the SEM images of the protected and nonprotected CL/D−P collagen, which showed fibril-like structures for protected collagen. It is possible that the presence of erythritol molecules affected the assembly of the helical strands and modified the collagen structure, from a triple helix-dominated structure to an alpha-helical one; however, this requires further investigation.

To further investigate the role of the charged amino acid in the triple helix formation, we obtained the CD spectrum of the CL domain at pH = 3 (Figure 3E). To do so, we first isolated the CL domain via trypsin digestion. The ellipticity value significantly dropped at 220 nm when the resulting CL domain was exposed to acidic pH compared with pH = 7. This reduction indicated that basic amino acids (aspartate and glutamate) play a significant role in triple helix formation for bacterial collagen and that their electrostatic interactions can be disrupted in acidic pH. We also studied the thermal unfolding curves of the purified samples at 198 nm between 5 °C and 50 °C (Figure S5). As the temperature increased, type-I animal collagen showed a significant change in the ellipticity value, indicating the transition from triple helix

https://doi.org/10.1021/acs.biomac.1c01191
Biomacromolecules 2022, 23, 1557−1568

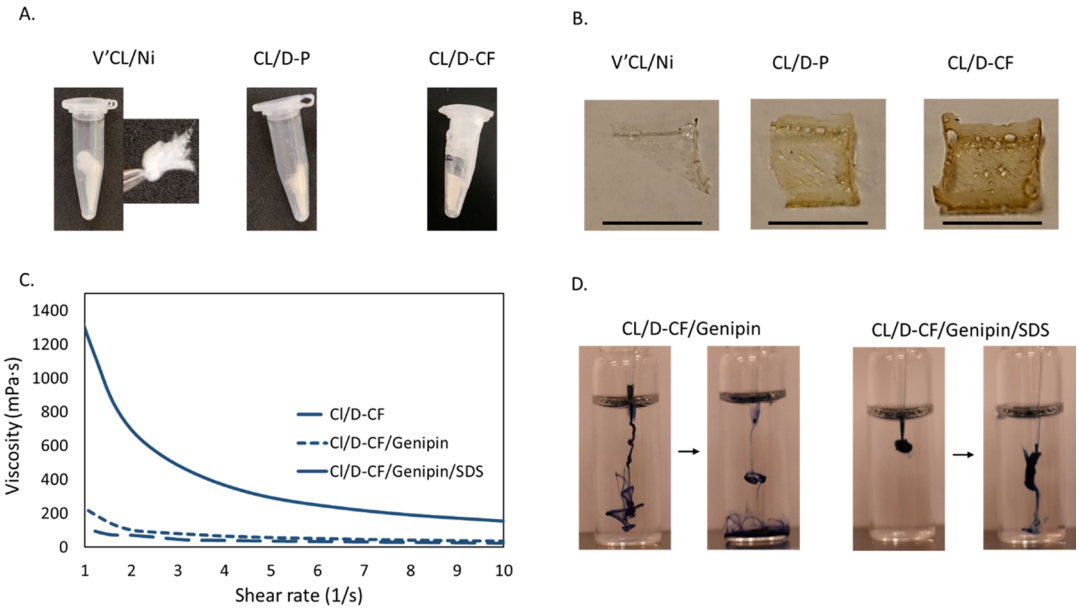

Figure 4. Bacterial collagen processed in different forms. (A) Dried collagen samples after purification with different methods and lyophilization. (B) Thin free-standing collagen films. Scale bar: 1 cm. (C) Viscosity of the genipin (5 mM) and SDS-treated collagen samples upon different shear rates indicating shear-thinning behavior of the collagen gels. (D) Snapshots of manual injections of collagen crosslinked with genipin and gelated with SDS into water.

at lower temperatures to random coil at higher temperatures (Figure S5A). The observed transition temperature (33 °C) was close to the previously reported melting temperature of type-I animal collagen.[42] We also observed a similar transition in the V′CL/Ni sample. According to the thermal unfolding curve, the V′CL/Ni sample started unfolding at around 25 °C (Figure S5B). The lower transition temperature can be explained by the smaller size of bacterial collagen compared with animal collagen and by the presence of the noncollagenous domains (N22, TEE, His-tag, V domain). Similarly, the V′CL/CF showed a slight change in the ellipticity value as temperature increased and started unfolding at around 25 °C. However, the purified samples that were exposed to the pepsin digestion and acid treatment (CL/D−P, CL/DP (erythritol), and CL/D−CF) showed no clear thermal transition, which is likely due to the partial denaturation and unfolding of these collagen samples during the purification processes (Figure S5C).

To further investigate chemical and conformational changes of the collagen samples after the purification processes, we obtained the Raman spectra of the collagen samples. Figure 4G shows the Raman spectra of the purified collagen molecules in the range of 1800−600 cm^{-1}, along with some relevant biomarkers and characteristic bands for type-I collagen. In all bacterial collagen samples, we observed a broad amide I band with a center typically around ∼1670 cm^{-1}. The amide I band is largely influenced by the vibrations of the backbone carbonyls, and its position can provide information about the specific conformation of the proteins in the sample. In this case, the position at 1670 cm^{-1} is consistent with an extended conformation, such as that would be observed in a triple helix, beta-turn, beta-sheet, or extended coil.[43,44] The vibrations at around 920 and 855 cm^{-1} likely arise from vibrations in the proline ring, reflecting the high proline content in bacterial collagen.[45−47] The amide III Raman band for proteins is located between 1200 and 1350 cm^{-1}, and the positions of the maxima are also influenced by the specific protein's conformations present in the sample. For example, the amide III bands of collagen typically consist of two major maxima at 1271 cm^{-1} (assigned to nonpolar fragments with a high proline content that form a typical collagen triple helix) and 1244 cm^{-1} (assigned to polar fragments of collagen characterized by a low proline content) with lower intensity at wavenumbers above 1300 cm^{-1}.[47] In the V′CL/Ni sample, two peaks of the amide III region appeared at 1230 and 1270 cm^{-1}, as expected.[46] However, in most of the other samples, the amide III bands exhibited two maxima at around 1310 and 1340 cm^{-1}, which is typically associated with an alpha-helical structure.[48] On the other hand, the amide I band position at ∼1670 cm^{-1} is inconsistent with the alpha-helical secondary structure, which is typically in the range of 1650−1655 cm^{-1}.[49] Thus, we are currently cautious not to overinterpret these spectra, with the implication that there may be a mixture of secondary structures in these particular samples, possibly owing to their different processing and purification methods utilized.

In summary, from the CD and Raman investigations, we conclude that the collagen obtained from Ni-NTA chromatography forms ordered triple helical structures and that the collagen purified via cross-flow filtration or acid precipitation is slightly more disordered, and in some cases may even contain an alpha-helical structure. The acidic processing steps (starting with pepsin digestion) may disrupt some of the interactions between collagen chains. It may be possible, however, to modify the purification processes to avoid compromising triple helix formation, by omitting the pepsin digestion step, and by protecting collagen against acids with erythritol.

Processing Bacterial Collagen. Finally, we wished to demonstrate that the secreted and purified collagen could be used to fabricate materials. To study the processability of the collagen samples, we formulated them into thin films and crosslinked hydrogels. First, freeze-dried collagen samples showed a sponge-like fibrous structure that could mimic the fibrous structure of type-I collagen (Figure 4A). Next, we prepared free-standing thin films of ∼0.2 mm thickness, by casting the collagen solution into the silicon molds (Figure 4B). Such films could be potentially be applied to wound healing and tissue engineering problems.[50] Because collagen possesses high biodegradability and morphological plasticity, it is capable of rebuilding the microenvironment of the wounded tissues and achieving infiltration of a variety of cells, neovascularization, and extracellular matrix deposition.[51]

Although collagen holds valued biochemical properties such as resistance to protease degradation, it requires physical or chemical modifications to improve its stability especially for in vivo applications. Therefore, we then used genipin to crosslink the collagen samples. Genipin can react with the primary amine groups of the collagen and form the cyclic structures that act as fluorophores. To confirm the successful genipin crosslinking reaction, we measured the absorbance and fluorescence of the crosslinked collagen materials. In the presence of oxygen, genipin-bound amines turn blue, and their absorbance at ∼590 nm increases (Figure S6A). The genipin-modified collagen

https://doi.org/10.1021/acs.biomac.1c01191
Biomacromolecules 2022, 23, 1557−1568

fluoresces at ~640 nm (Figure S6B). We observed increased absorbance and fluorescence intensities with increasing genipin-to-collagen ratio, also yielding more crosslink points. To further induce the gelation of the collagen, we used SDS, a low-molecular-weight surfactant. The rapid SDS-induced gelation of silk and curli proteins has been reported previously.[52,53] Indeed, the presence of the SDS can provide hydrophobic interactions and intensify the electrostatic interactions between the charged residues of the collagen molecules and their negative charge.

To investigate the effect of the genipin crosslinking and SDS gelation on collagen viscosity, we measured the viscosity of the genipin- and SDS-treated samples under different shear rates (Figure 4C). Upon crosslinking, although strong chemical bonds between collagen molecules can be formed, which strengthens the intramolecular and intermolecular interactions between collagen fibers, the viscosity of the sample did not change significantly. An important factor for injectability is to determine whether the hydrogel is shear-thinning. Shear-thinning hydrogels experience decreases in viscosity upon application of shear stress, which we observed in the SDS-induced gelated collagen (Figure 4C). We also illustrated collagen gelation by presenting snapshots of manual injections of genipin and SDS-treated collagen solutions into water (Figure 4D). The genipin-treated collagen showed rapid dispersion immediately after injection, while the SDS-gelated collagen maintained its material integrity after injection.

CONCLUSIONS

Depending on the purification and processing, recombinantly produced bacterial collagen can possess structural stability and conformation features (e.g., triple helix) comparable to type-I animal collagen with emerging uses as biomaterials for a broad range of applications. Herein, inspiration from the extracellular secretion system for curli fibers allows us to engineer a simple secretion pathway for bacterial collagen in *E. coli* cells. Most importantly, the extracellular secretion prevented the need for cell rupture, and therefore, simplified the isolation of bacterial collagen. After simply centrifuging the bacterial culture, the crude supernatant itself exhibited a close to 50% collagen content. Then, using cost-effective and simple purification methods, we obtained more than 90% purity and around 0.4 g/L purification yield, in a fast and easy manner.

Analysis of the morphology and secondary structure of the collagen products indicated that the secreted and purified bacterial collagen formed fibrillar structures similar to type-I animal collagen. While the structure of bacterial collagen differs slightly from that of type-I collagen, as it is held together by pairs of charged residues, they share many structural and physicochemical characteristics. Under the right conditions, secreted bacterial collagen was able to form elongated triple helical structures of hundreds of nanometers in length, held together by electrostatic interactions. We also demonstrated that bacterial collagen can be processed as dried proteins, films, and crosslinked hydrogels, all of which can enable the utilization of collagen as the main component of functional biomaterials.

ASSOCIATED CONTENT

Supporting Information

The Supporting Information is available free of charge at https://pubs.acs.org/doi/10.1021/acs.biomac.1c01191.

Protein sequence of bacterial collagen and DNA sequences of the genes, abbreviation table, distribution of the collagen obtained from the pET21d-*v′cl-csgEG* and pET21d-*v′cl-csgEFG* vectors *via* Western Blotting, Sirius Red stained cultures expressing the pET21d-*v′cl-csgEG* and pET21d-*v′cl-csgEFG* vectors, Masson's trichrome staining, thermal transitions of the purified proteins from circular dichroism, absorbance and fluorescence emission spectra of the genipin-crosslinked samples (PDF)

AUTHOR INFORMATION

Corresponding Author

Noémie-Manuelle Dorval Courchesne − *Department of Chemical Engineering, McGill University, Montreal H3A 0C5 Quebec, Canada*; orcid.org/0000-0002-3589-3545; Email: Noemie.dorvalcourchesne@mcgill.ca

Authors

Zahra Abdali − *Department of Chemical Engineering, McGill University, Montreal H3A 0C5 Quebec, Canada*

Max Renner-Rao − *Department of Chemistry, McGill University, Montreal H3A 0C5 Quebec, Canada*

Amy Chow − *Department of Chemical Engineering, McGill University, Montreal H3A 0C5 Quebec, Canada*

Anqi Cai − *Department of Chemical Engineering, McGill University, Montreal H3A 0C5 Quebec, Canada*

Matthew J. Harrington − *Department of Chemistry, McGill University, Montreal H3A 0C5 Quebec, Canada*; orcid.org/0000-0003-1417-9251

Complete contact information is available at: https://pubs.acs.org/10.1021/acs.biomac.1c01191

Author Contributions

Z. A.: Conceptualization, methodology, investigation, writing—original draft, and visualization. M. R.: Methodology and investigation. A. C.: Investigation. A. C.: Investigation. M. J. H.: Methodology, writing-reviewing, and editing. N.-M.D. C.: Supervision, conceptualization, methodology, writing-reviewing and editing, and funding acquisition.

Funding

This research was funded, in part, by the Natural Sciences and Engineering Research Council of Canada (NSERC) through a Discovery grant (NSERC RGPIN-2017-04598), by the Fonds de Recherche du Quebec − Nature et Technologies (FRQNT), and it was undertaken, thanks to the support by the Canadian Foundation for Innovation (project #37524). Z.A. is grateful for financial support via a McGill Engineering Doctoral Award (MEDA) and an FRQNT Doctoral Research Scholarship, and A.C. is grateful for a McGill Engineering Undergraduate Student Masters Award (MEUSMA).

Notes

The authors declare the following competing financial interest(s): Zahra Abdali and Noémie-Manuelle Dorval Courchesne are co-inventors on a continuation-in-part of U.S. patent application No. 15/776, 998.

ACKNOWLEDGMENTS

The authors thank the Facility for Electron Microscopy and Research (FEMR) at McGill for assistance with SEM, the McGill Chemistry Microscopy and Imaging Lab (MIlab) for providing AFM facility, and Dr. Jason Young's lab at McGill (Department of Biochemistry) and Dr. Hanadi Sleiman at McGill (Department of Chemistry) for the use of their circular dichroism spectrometers.

REFERENCES

(1) Fertala, A. Three Decades of Research on Recombinant Collagens: Reinventing the Wheel or Developing New Biomedical Products? *Bioengineering* **2020**, *7*, 155.

(2) Parenteau-Bareil, R.; Gauvin, R.; Berthod, F. Collagen-Based Biomaterials for Tissue Engineering Applications. *Materials* **2010**, *3*, 1863.
(3) Lukomski, S.; Nakashima, K.; Abdi, I.; Cipriano, V. J.; Shelvin, B. J.; Graviss, E. A.; Musser, J. M. Identification and characterization of a second extracellular collagen-like protein made by group A Streptococcus: control of production at the level of translation. *Infect. Immun.* **2001**, *69*, 1729.
(4) Xu, Y.; Keene, D. R.; Bujnicki, J. M.; Hook, M.; Lukomski, S. Streptococcal Scl1 and Scl2 proteins form collagen-like triple helices. *J. Biol. Chem.* **2002**, *277*, 27312.
(5) Mohs, A.; Silva, T.; Yoshida, T.; Amin, R.; Lukomski, S.; Inouye, M.; Brodsky, B. Mechanism of stabilization of a bacterial collagen triple helix in the absence of hydroxyproline. *J. Biol. Chem.* **2007**, *282*, 29757.
(6) An, B.; DesRochers, T. M.; Qin, G.; Xia, X.; Thiagarajan, G.; Brodsky, B.; Kaplan, D. L. The influence of specific binding of collagen-silk chimeras to silk biomaterials on hMSC behavior. *Biomaterials* **2013**, *34*, 402.
(7) Seo, N.; Russell, B. H.; Rivera, J. J.; Liang, X.; Xu, X.; Afshar-Kharghan, V.; Hook, M. An engineered alpha1 integrin-binding collagenous sequence. *J. Biol. Chem.* **2010**, *285*, 31046.
(8) Merrett, K.; Wan, F.; Lee, C. J.; Harden, J. L. Enhanced Collagen-like Protein for Facile Biomaterial Fabrication. *ACS Biomater. Sci. Eng.* **2021**, *7*, 1414.
(9) O'Leary, L. E.; Fallas, J. A.; Bakota, E. L.; Kang, M. K.; Hartgerink, J. D. Multi-hierarchical self-assembly of a collagen mimetic peptide from triple helix to nanofibre and hydrogel. *Nat. Chem.* **2011**, *3*, 821−828.
(10) Fallas, J. A.; Dong, J.; Tao, Y. J.; Hartgerink, J. D. Structural insights into charge pair interactions in triple helical collagen-like proteins. *J. Biol. Chem.* **2012**, *287*, 8039.
(11) Peng, Y. Y.; Stoichevska, V.; Madsen, S.; Howell, L.; Dumsday, G. J.; Werkmeister, J. A.; Ramshaw, J. A. A simple cost-effective methodology for large-scale purification of recombinant non-animal collagens. *Appl. Microbiol. Biotechnol.* **2014**, *98*, 1807.
(12) Choi, J. H.; Lee, S. Y. Secretory and extracellular production of recombinant proteins using Escherichia coli. *Appl. Microbiol. Biotechnol.* **2004**, *64*, 625.
(13) Su, L.; Xu, C.; Woodard, R. W.; Chen, J.; Wu, J. A novel strategy for enhancing extracellular secretion of recombinant proteins in *Escherichia coli*. *Appl. Microbiol. Biotechnol.* **2013**, *97*, 6705.
(14) Barnhart, M. M.; Chapman, M. R. Curli biogenesis and function. *Annu. Rev. Microbiol.* **2006**, *60*, 131.
(15) Blanco, L. P.; Evans, M. L.; Smith, D. R.; Badtke, M. P.; Chapman, M. R. Diversity, biogenesis and function of microbial amyloids. *Trends Microbiol.* **2012**, *20*, 66.
(16) Dorval Courchesne, N. M.; Duraj-Thatte, A.; Tay, P. K. R.; Nguyen, P. Q.; Joshi, N. S. Scalable Production of Genetically Engineered Nanofibrous Macroscopic Materials via Filtration. *ACS Biomater. Sci. Eng.* **2017**, *3*, 733.
(17) Nenninger, A. A.; Robinson, L. S.; Hammer, N. D.; Epstein, E. A.; Badtke, M. P.; Hultgren, S. J.; Chapman, M. R. CsgE is a curli secretion specificity factor that prevents amyloid fibre aggregation. *Mol. Microbiol.* **2011**, *81*, 486.
(18) Nenninger, A. A. Localized and efficient curli nucleation requires the chaperone-like amyloid assembly protein CsgF. *PNAS* **2009**, *106*, 900.
(19) Goyal, P.; Krasteva, P. V.; Van Gerven, N.; Gubellini, F.; Van den Broeck, I.; Troupiotis-Tsailaki, A.; Jonckheere, W.; Pehau-Arnaudet, G.; Pinkner, J. S.; Chapman, M. R.; Hultgren, S. J.; Howorka, S.; Fronzes, R.; Remaut, H. Structural and mechanistic insights into the bacterial amyloid secretion channel CsgG. *Nature* **2014**, *516*, 250.
(20) Van Gerven, N.; Goyal, P.; Vandenbussche, G.; De Kerpel, M.; Jonckheere, W.; De Greve, H.; Remaut, H. Secretion and functional display of fusion proteins through the curli biogenesis pathway. *Mol. Microbiol.* **2014**, *91*, 1022.
(21) Abdali, Z.; Aminzare, M.; Zhu, X.; DeBenedictis, E.; Xie, O.; Keten, S.; Dorval Courchesne, N. M. Curli-Mediated Self-Assembly of a Fibrous Protein Scaffold for Hydroxyapatite Mineralization. *ACS Synth. Biol.* **2020**, *9*, 3334.
(22) Taylor, J. D.; Zhou, Y.; Salgado, P. S.; Patwardhan, A.; McGuffie, M.; Pape, T.; Grabe, G.; Ashman, E.; Constable, S. C.; Simpson, P. J.; Lee, W. C.; Cota, E.; Chapman, M. R.; Matthews, S. J. Atomic resolution insights into curli fiber biogenesis. *Structure* **2011**, *19*, 1307.
(23) Delgado, L. M.; Shologu, N.; Fuller, K.; Zeugolis, D. I. Acetic acid and pepsin result in high yield, high purity and low macrophage response collagen for biomedical applications. *Biomed. Mater.* **2017**, *12*, 065009.
(24) Qing, G.; Ma, L. C.; Khorchid, A.; Swapna, G. V.; Mal, T. K.; Takayama, M. M.; Xia, B.; Phadtare, S.; Ke, H.; Acton, T.; Montelione, G. T.; Ikura, M.; Inouye, M. Cold-shock induced high-yield protein production in Escherichia coli. *Nat. Biotechnol.* **2004**, *22*, 877.
(25) Johnston, N.; Dettmar, P. W.; Bishwokarma, B.; Lively, M. O.; Koufman, J. A. Activity/stability of human pepsin: implications for reflux attributed laryngeal disease. *Laryngoscope* **2007**, *117*, 1036.
(26) Meredith, S. C. The determination of molecular weight of proteins by gel permeation chromatography in organic solvents. *J. Biol. Chem.* **1984**, *259*, 11682.
(27) Rittié, L. Method for Picrosirius Red-Polarization Detection of Collagen Fibers in Tissue Sections. *Methods Mol. Biol.* **2017**, *1627*, 395.
(28) Kliment, C. R.; Englert, J. M.; Crum, L. P.; Oury, T. D. A novel method for accurate collagen and biochemical assessment of pulmonary tissue utilizing one animal. *Int. J. Clin. Exp. Pathol.* **2011**, *4*, 349.
(29) Lee, H. J.; Lee, J. S.; Chansakul, T.; Yu, C.; Elisseeff, J. H.; Yu, S. M. Collagen mimetic peptide-conjugated photopolymerizable PEG hydrogel. *Biomaterials* **2006**, *27*, 5268.
(30) Ueda, E. K. M.; Gout, P. W.; Morganti, L. Current and prospective applications of metal ion−protein binding. *J. Chromatogr. A* **2003**, *988*, 1−23.
(31) Li, Y.; Asadi, A.; Monroe, M. R.; Douglas, E. P. pH effects on collagen fibrillogenesis in vitro: Electrostatic interactions and phosphate binding. *Mater. Sci. Eng. C* **2009**, *29*, 1643.
(32) Usha, R.; Raman, S. S.; Subramanian, V.; Ramasami, T. Role of polyols (erythritol, xylitol and sorbitol) on the structural stabilization of collagen. *Chem. Phys. Lett.* **2006**, *430*, 391.
(33) Li, F.; Ducker, M.; Sun, B.; Szele, F. G.; Czernuszka, J. T. Interpenetrating polymer networks of collagen, hyaluronic acid, and chondroitin sulfate as scaffolds for brain tissue engineering. *Acta Biomater.* **2020**, *112*, 122.
(34) Sarkar, B.; O'Leary, L. E.; Hartgerink, J. D. Self-assembly of fiber-forming collagen mimetic peptides controlled by triple-helical nucleation. *J. Am. Chem. Soc.* **2014**, *136*, 14417.
(35) Kohler, M.; Marchand, A.; Hentzen, N. B.; Egli, J.; Begley, A. I.; Wennemers, H.; Zenobi, R. Temperature-controlled electrospray ionization mass spectrometry as a tool to study collagen homo- and heterotrimers. *Chem. Sci.* **2019**, *10*, 9829.
(36) Shyam Rele, Y. S.; Apkarian, R. P.; Zheng, Q.; Conticello, V. P.; Chaikof, E. L. D-Periodic Collagen-Mimetic Microfibers. *J. Am. Chem. Soc.* **2007**, *129*, 14780.
(37) Tanrikulu, I. C.; Forticaux, A.; Jin, S.; Raines, R. T. Peptide tessellation yields micrometre-scale collagen triple helices. *Nat. Chem.* **2016**, *8*, 1008.
(38) Hulgan, S. A. H.; Jalan, A. A.; Li, I. C.; Walker, D. R.; Miller, M. D.; Kosgei, A. J.; Xu, W.; Phillips, G. N., Jr.; Hartgerink, J. D. Covalent Capture of Collagen Triple Helices Using Lysine-Aspartate and Lysine-Glutamate Pairs. *Biomacromolecules* **2020**, *21*, 3772.
(39) Drzewiecki, K. E.; Grisham, D. R.; Parmar, A. S.; Nanda, V.; Shreiber, D. I. Circular Dichroism Spectroscopy of Collagen Fibrillogenesis: A New Use for an Old Technique. *Biophys. J.* **2016**, *111*, 2377.
(40) Xu, C.; Yu, Z.; Inouye, M.; Brodsky, B.; Mirochnitchenko, O. Expanding the family of collagen proteins: recombinant bacterial collagens of varying composition form triple-helices of similar stability. *Biomacromolecules* **2010**, *11*, 348−356.
(41) Wei, Y.; Thyparambil, A. A.; Latour, R. A. Protein helical structure determination using CD spectroscopy for solutions with strong background absorbance from 190 to 230nm. *Biochim. Biophys. Acta* **2014**, *1844*, 2331.

https://doi.org/10.1021/acs.biomac.1c01191
Biomacromolecules 2022, 23, 1557−1568

(42) Leikina, E.; Mertts, M. V.; Kuznetsova, N.; Leikin, S. Type I collagen is thermally unstable at body temperature. *PNAS* **2002**, *99*, 1314−1318.
(43) Frushour, B. G. Raman Scattering of Collagen, Gelatin, and Elastin. *Biopolymers* **1975**, *14*, 379.
(44) Lefevre, T.; Paquet-Mercier, F.; Rioux-Dube, J. F.; Pezolet, M. Review structure of silk by raman spectromicroscopy: from the spinning glands to the fibers. *Biopolymers* **2012**, *97*, 322.
(45) Khalid, M.; Bora, T.; Ghaithi, A. A.; Thukral, S.; Dutta, J. Raman Spectroscopy detects changes in Bone Mineral Quality and Collagen Cross-linkage in Staphylococcus Infected Human Bone. *Sci. Rep.* **2018**, *8*, 9417.
(46) Ikoma, T.; Kobayashi, H.; Tanaka, J.; Walsh, D.; Mann, S. Physical properties of type I collagen extracted from fish scales of Pagrus major and Oreochromis niloticas. *Int. J. Biol. Macromol.* **2003**, *32*, 199.
(47) Olsztyńska-Janus, S.; Szymborska-Małek, K.; Gąsior-Głogowska, M.; Walski, T.; Komorowska, M.; Witkiewicz, W.; Pezowicz, C.; Kobielarz, M.; Szotek, S. Spectroscopic techniques in the study of human tissues and their components. Part II: Raman spectroscopy. *Acta Bioeng. Biomech.* **2012**, *14*, 101.
(48) Mikhonin, A. V.; Bykov, S. V.; Myshakina, N. S.; Asher, S. A. Peptide Secondary Structure Folding Reaction Coordinate: Correlation between UV Raman Amide III Frequency, Ψ Ramachandran Angle, and Hydrogen Bonding. *J. Phys. Chem. B* **2006**, *110*, 1928.
(49) Bandekar, J. Amide modes and protein conformation. *Biochim. Biophys. Acta* **1992**, *1120*, 123.
(50) Chattopadhyay, S.; Raines, R. T. Review collagen-based biomaterials for wound healing. *Biopolymers* **2014**, 821.
(51) Long, G.; Liu, D.; He, X.; Shen, Y.; Zhao, Y.; Hou, X.; Chen, B.; OuYang, W.; Dai, J.; Li, X. A dual functional collagen scaffold coordinates angiogenesis and inflammation for diabetic wound healing. *Biomater. Sci.* **2020**, *8*, 6337.
(52) Wu, X.; Hou, J.; Li, M.; Wang, J.; Kaplan, D. L.; Lu, S. Sodium dodecyl sulfate-induced rapid gelation of silk fibroin. *Acta Biomater.* **2012**, *8*, 2185−2192.
(53) Duraj-Thatte, A. M.; Dorval Courchesne, N.-M.; Praveschotinunt, P.; Rutledge, J.; Lee, Y.; Karp, J. M.; Joshi, N. S. Genetically Programmable Self-Regenerating Bacterial Hydrogels. *Adv. Mater.* **2019**, *31*, No. 1901826.

https://doi.org/10.1021/acs.biomac.1c01191
Biomacromolecules 2022, 23, 1557−1568